Proceedings of 2014 Workshop on Fundamental Issues and Future Research Directions for Parallel Mechanisms and Manipulators
July 7–8, 2014, Tianjin, China

A Completely Kinematostatically Decoupled XY Compliant Parallel Manipulator through a New Topology Structure

Guangbo Hao[1]*, Jingjun Yu[2]
[1]School of Engineering, University College Cork, Cork, Ireland
[2]School of Mechanical Engineering and Automation, Beihang University, Beijing, 100191, China
*e-mail: G.Hao@ucc.ie

Abstract: This paper deals with a completely kinematostaticaly decoupled XY compliant parallel manipulator (CPM) composed of exactly-constrained compliant modules. A new 4-PP XY translational parallel mechanism (TPM) with a new topology structure is firstly proposed where each two P (P: prismatic) joints on the base in two non-adjacent legs are rigidly connected. A novel 4-PP XY CPM is then obtained by replacing each traditional P join on the base in the 4-PP XY TPM with a compound basic parallelogram module (CBPM) and replacing each traditional P joint on the motion stage with a basic parallelogram module (BPM). Approximate analytical model is derived with comparison to the FEA (finite element analysis) model and experiment for a case study. The proposed novel XY CPM has a compact configuration with good dynamics, and is able to well constrain the parasitic rotation and the cross-axis coupling of the motion stage. The cross-axis motion of the input stage can be completely eliminated, and the lost motion between the input stage and the motion stage is significantly reduced.

Keywords: Compliant parallel manipulator; Complete decoupling; Exact constraint; Analytical modeling; Topology structure

1 Introduction

XY compliant parallel manipulators (CPMs) have been extensively used in a variety of applications such as the atomic force microscope [1, 2], micro-assembly [3] and data storage [4], which transfer motion/load through the deformation of flexible members (i.e. flexure mechanisms) and are parallel-type manipulators. Their merits include eliminated backlash and friction, no need for lubrication, reduced wear and noise, and monolithic configuration [5].

It is always desired to design completely kinematostaticaly decoupled XY CPMs in order to simplify the high-precision motion control [6]. Here, kinematostatic decoupling means that one primary output translational displacement of the motion stage is only affected by the actuation force on the input stage along the same direction, which describes the relationship between the input force and output motion. It is referred to cross-axis coupling of the output motion stage if the output displacement along one axis is affected by the force along another axis. Apart from the output translational displacement, the input force on one input stage should not cause any cross-axis motion of another input stage (if not positioned by the linear actuator). In order to achieve kinematostatic decoupling, geometrical decoupling [7] is necessary at first. Based on the geometrically decoupled 2-PP (P: prismatic joint) XY TPM (translational parallel mechanism) and 4-PP XY TPM [8], XY CPMs with geometrical decoupling can be obtained by replacing each traditional P joint with an appropriate flexural counterpart. It is noted that the 4-PP XY CPM is better for minimizing the parasitic rotation of the motion stage, where four compliant P joints are directly connected to the base (on the base) with two of them actuated, and the other four P joints are directly connected to the output motion stage (on the motion stage).

Four types of commonly-used parallelogram based compliant P joints with distributed compliance (Fig. 1) have been often employed to propose geometrically decoupled 4-PP XY CPMs with mirror symmetry [9-11] or rotational symmetry [6].

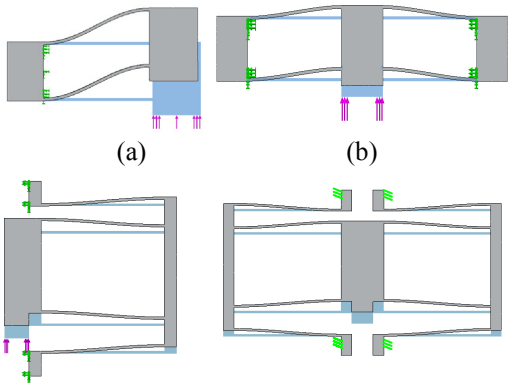

Figure 1 Four types of parallelogram based compliant P joints: (a) basic parallelogram module (BPM); (b) compound basic parallelogram module (CBPM) composed of two BPMs in mirror symmetry; (c) double parallelogram module (DPM); (d) compound double parallelogram module (CDPM) composed of two DPMs in mirror symmetry

However, these emerging XY CPMs still have their own limitations/shortcomings. The 4-PP XY CPMs using DPMs and/or CDPMs as compliant P joints reported in [6, 9] can cause poor dynamic performance due to the under-constrained design (the non-controllable secondary motion mass) [8-9]. The dramatic off-axis stiffness degradation of the DPM or CDPM [12] because of the secondary motion mass has also the negative influence on the performance characteristics of the XY CPMs. The XY CPM in [10] was proposed by replacing each P joint directly connected

to the base with a CBPM, and replacing each P joint directly connected to motion stage with a BPM. But the input force on the input stage inevitably brings the cross-axis motion of another input stage due to the relatively large parasitic translation from the BPM [8]. Li et al [11] eliminated this cross-axis motion of the input stage for the proposed 4-PP XY CPM by using the CBPM instead of the BPM as the compliant P joint directly connected to the motion stage. But this strategy can result in a bulky configuration without any improvements on reduced lost motion and reduced parasitic rotation over the design in [10].

Building on the above advances, this paper aims to design a completely kinematostatically decoupled XY CPM composed of exactly-constrained compliant modules, BPMs, based on a new topology structure. This paper is organized as follows. Section 2 proposes a novel 4-PP XY CPM based on a new topology structure. Kinematostatic modeling is carried out in Section 3. A case study is detailed in Section 4 followed by further discussions in Section 5. Conclusions are finally drawn.

2 Design of a Completely Decoupled XY CPM

2.1 New 4-PP TPM topology structure

A new 4-PP TPM topology structure is presented in Fig. 2, which is fully symmetric and geometrically decoupled. It is composed of four PP legs (Legs 1, 2, 3, and 4) in one plane. Each PP leg is composed of two P joints perpendicular to each other in series. The directions of two adjacent P joints on the motion stage are perpendicular to each other. The two P joints on the base in Legs 1 and 3 (two non-adjacent legs) are rigidly connected together, as are the two P joints on the base in Legs 2 and 4 so that the P joints on the base are actuated joints and the P joints on the motion stage are passive joints.

It will be seen in the next section that the new 4-PP TPM topology structure is capable of producing kinematostaticaly decoupled XY CPM.

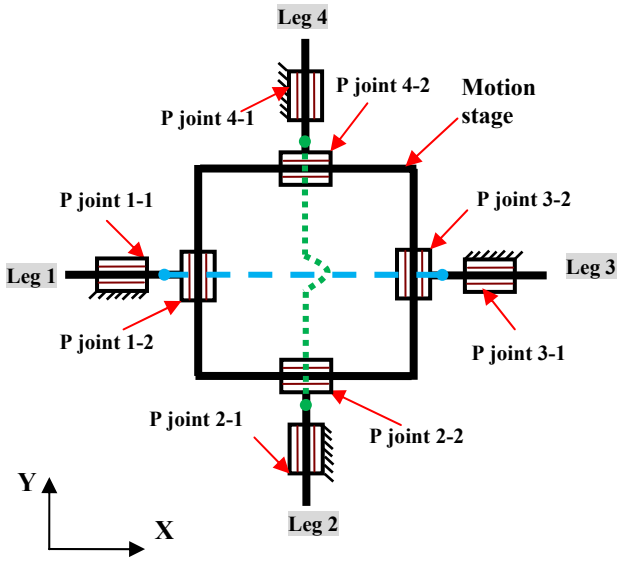

Figure 2 New 4-PP TPM topology structure

2.2 Novel 4-PP XY CPM

A completely decoupled XY CPM (Fig. 3) can be obtained based on the new 4-PP TPM topology structure (Fig. 2). This is done by replacing each traditional P joint on the base with the CBPM, and replacing each traditional P joint on the motion stage with the BPM. It can be observed that the novel 4-PP XY CPM can be regarded to consist of six CBPMs with three in each axis.

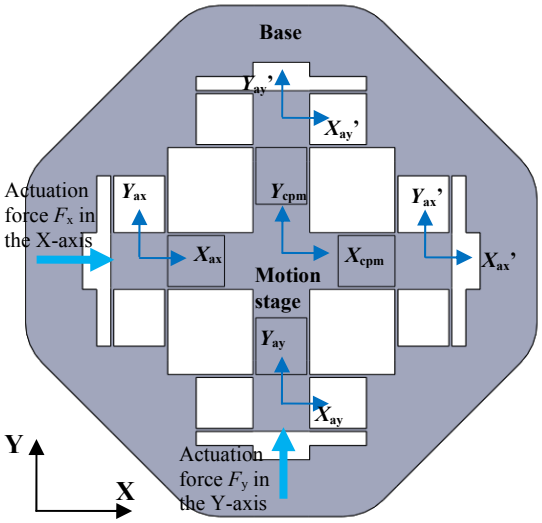

(a) XY CPM view I: Top view

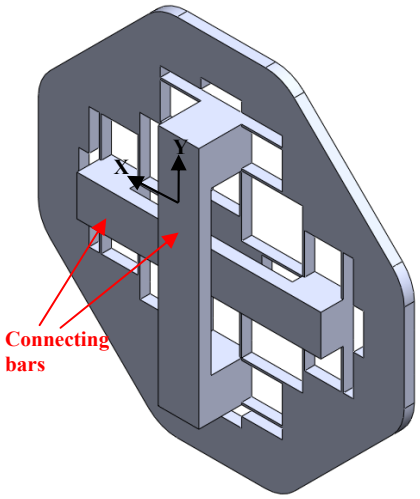

(b) XY CPM view II: Isometric view

Figure 3 A novel 4-PP XY CPM

It is noted that the proposed novel XY CPM has a compact configuration without non-controllable mass, and can well constrain the parasitic rotation and the cross-axis coupling of the motion stage due to the fully symmetric design. The cross-axis motion of the input stage by the input force imposed on another input stage can be completely eliminated due to the symmetric structure and the rigid connection between the compliant P joints on the base in two non-adjacent legs. Moreover, the lost motion between the input stage and the motion stage is significantly reduced since the passive P joint suffers from lower internal tensile loading and has a relatively large off-axis stiffness, which can further alleviate the parasitic rotation of the motion stage.

3 Kinematostatic Modelling

In this section, kinematostatic modeling is conducted to capture the load-displacement relationships of the novel 4-PP XY CPM. Note that normalization strategy is employed throughout the derivations in this section, which refers to that all translational displacements and length parameters are normalized by the beam actual length L, forces by EI/L^2, and moments by EI/L. Here, E denotes the Young's modulus, and I represents the second moment of the area of a rectangular cross section. All of the normalized parameters are denoted by the corresponding lower-case letters.

The translational displacements (x_s and y_s) for the CBPM are first derived under the given forces of f_y and p (Fig. 4) when neglecting the trivial contribution from the parasitic rotational yaw. Based on the definition of the internal forces in BPM1 and BPM2 in Fig. 4 and the load-displacement equations of the BPM derived by Awtar [13], we can have the following four equations with four unknown variables (internal forces):

$$\begin{cases} y_s = \dfrac{f_{y1}}{24+1.2p_1} = \dfrac{f_{y2}}{24+1.2p_2} \\ x_s = \dfrac{p_1}{2d} - 0.6y_s^2 + \dfrac{p_1}{1400}y_s^2 = -(\dfrac{p_2}{2d} - 0.6y_s^2 + \dfrac{p_2}{1400}y_s^2) \\ f_{y1} + f_{y2} = f_y \\ p_1 - p_2 = p \end{cases} \tag{1}$$

where $d=12/(T/L)^2$. T is the beam in-plane thickness.

The solutions to Eq. (1) can be derived as

$$\begin{cases} p_1 = \dfrac{1.2y_s^2 + p/2d + py_s^2/1400}{1/d + y_s^2/700} = \dfrac{1.2y_s^2}{1/d + y_s^2/700} + \dfrac{p}{2} \\ p_2 = \dfrac{1.2y_s^2 - p/2d - py_s^2/1400}{1/d + y_s^2/700} = \dfrac{1.2y_s^2}{1/d + y_s^2/700} - \dfrac{p}{2} \\ f_{y1} = \dfrac{24+1.2(\dfrac{1.2y_s^2}{1/d+y_s^2/700} + \dfrac{p}{2})}{24+1.2(\dfrac{1.2y_s^2}{1/d+y_s^2/700})}\dfrac{f_y}{2} \\ f_{y2} = \dfrac{24+1.2(\dfrac{1.2y_s^2}{1/d+y_s^2/700} - \dfrac{p}{2})}{24+1.2(\dfrac{1.2y_s^2}{1/d+y_s^2/700})}\dfrac{f_y}{2} \end{cases} \tag{2}$$

Combining Eqs. (1) and (2), we have

$$x_s = p(\frac{1}{4d} + \frac{1}{2800}y_s^2) \tag{3}$$

$$y_s = \frac{f_y}{48+1.2(p_1+p_2)} = \frac{f_y}{48+1.2(\dfrac{2.4y_s^2}{1/d+y_s^2/700})} \tag{4}$$

Equation (3) shows that the primary motion displacement degrades the stiffness along the X-axis. Equation (4) implies that the tensile force p on the CBPM does not affect the primary motion stiffness that varies with the primary motion displacement only.

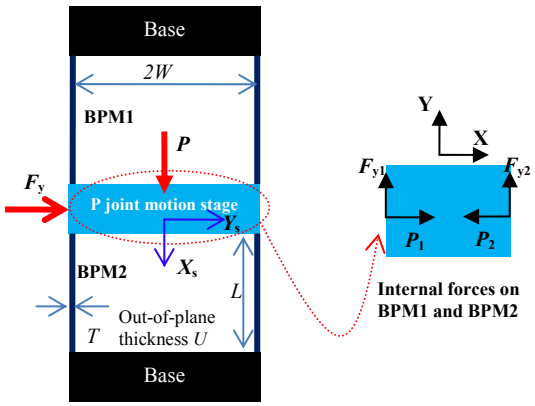

Figure 4 A CBPM with geometry and loading indication

Therefore, the analytical translational displacements of the motion stage of the novel 4-PP CPM can be approximately derived based on Eq. (4) and Fig. 4 as below:

$$\begin{cases} x_{cpm} = \dfrac{f_x/3}{48+1.2(\dfrac{2.4x_{cpm}^2}{1/d+x_{cpm}^2/700})} = \dfrac{f_x}{144+(\dfrac{8.64x_{cpm}^2}{1/d+x_{cpm}^2/700})} \\ y_{cpm} = \dfrac{f_y/3}{48+1.2(\dfrac{2.4y_{cpm}^2}{1/d+y_{cpm}^2/700})} = \dfrac{f_y}{144+(\dfrac{8.64y_{cpm}^2}{1/d+y_{cpm}^2/700})} \end{cases} \tag{5}$$

where x_{cpm} and y_{cpm} are the translational displacements of the motion stage of the novel 4-PP XY CPM along the X- and Y-axes, respectively. f_x and f_y are the two input forces exerted on the two input stages along the X- and Y-axes, respectively. Note that the results in Eq. (5) are obtained based on the assumptions that the displacements for different points on each connecting bar (input stage) are same (i.e. $y_{ay} = y_{ay}$' and $x_{ax} = x_{ax}$'), that the input stage's off-axis displacements are zero (i.e. $y_{ax} = y_{ax}$' $= x_{ay} = x_{ay}$'$=$ 0), that the cross-axis coupling motion of the motion stage is ignored, and that there is no lost motion between the input stage and the motion stage (i.e. $x_{ax} = x_{cpm}$ and $y_{ay} = y_{cpm}$).

Based on Eq. (5), we can obtain the analytical stiffness equations along both axes at the specific displacements:

$$\begin{cases} k_{x-cpm} = \dfrac{df_x}{dx_{cpm}} = 144 + \dfrac{25.92x_{cpm}^2}{(\dfrac{1}{d}+\dfrac{x_{cpm}^2}{700})} - \dfrac{17.28x_{cpm}^4}{700(\dfrac{1}{d}+\dfrac{x_{cpm}^2}{700})^2} \\ k_{y-cpm} = \dfrac{df_y}{dy_{cpm}} = 144 + \dfrac{25.92y_{cpm}^2}{(\dfrac{1}{d}+\dfrac{y_{cpm}^2}{700})} - \dfrac{17.28y_{cpm}^4}{700(\dfrac{1}{d}+\dfrac{y_{cpm}^2}{700})^2} \end{cases} \tag{6}$$

It can be found from Eq. (5) that the stiffness of the novel 4-PP XY CPM increases with the motion (i.e. load-stiffening effect) due to the introduced nonlinear terms, $(\dfrac{8.64x_{cpm}^2}{1/d+x_{cpm}^2/700})$ and $(\dfrac{8.64y_{cpm}^2}{1/d+y_{cpm}^2/700})$, in the denominator. If the nonlinear terms are not taken into account, the load-displacement equations for the novel XY CPM are the

linear models with a constant stiffness of 144 along each axis.

Equations (5) and (6) are plotted in Figs. 5 and 6 to show how the displacement (x_{cpm} or y_{cpm}) and the parameter d affect the required actuation force (f_x or f_y) and the stiffness ($k_{x\text{-}cpm}$ or $k_{y\text{-}cpm}$) over the normalized motion range of 0.1. It is shown that the larger d, the higher force and stiffness.

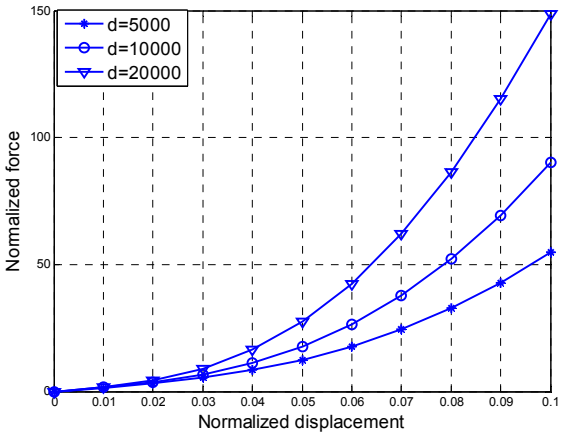

Figure 5 Normalized force against normalized displacement

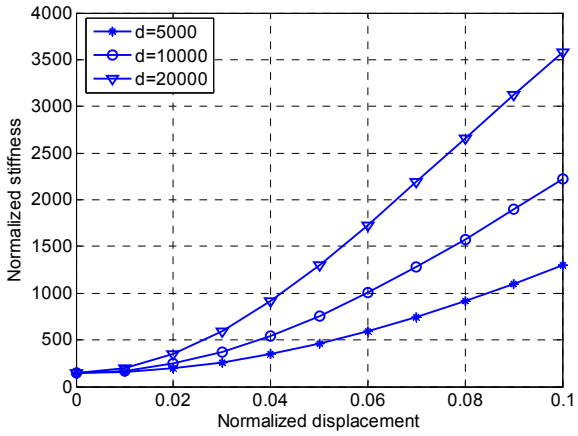

Figure 6 Normalized stiffness against normalized displacement

4 Case Study

Let all the CBPMs be identical with U=5 mm, W=10mm, T=1 mm, L=20 mm and 10 mm out-of-plane thickness for the connecting bars, and the nominal peripheral dimension of the XY CPM be 120 mm × 120 mm. The material of ABS Plus with a Young's Modulus of 2.32 GPa is selected for a case study. Nonlinear FEA is carried out in this paper with the two-axis forces limited to 0–20 N.

A physical prototype made of ABS Plus with the above geometry is printed for our initial experimental testing as shown in Fig. 7. This is done by a 3D printer, Dimension Elite, with a 178 μm resolution. Single-axis loading testing is implemented with the displacement measured by a low-force digital indicator with a motion resolution of 0.001 mm and a spring force of 0.4–0.7 N (Digimatic Indicator, Mitutoyo Corporation, Japan).

The input stage displacements (Y_{ay}') under single-axis loading along the Y-axis are shown in Fig. 8. It can be seen that the analytical result of the force under the same specified displacement is much larger than the nonlinear FEA result and much larger than the experiment result. However, all of the results indicate the load-stiffening effect (nonlinear stiffness).

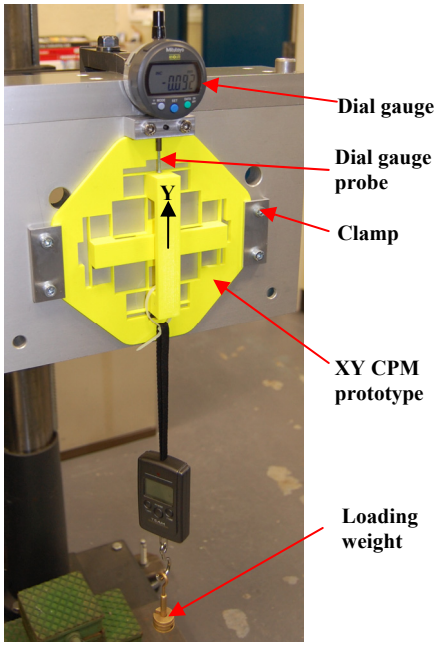

Figure 7 Single-axis loading testing rig

The lost motion and the input stage's off-axis translation using nonlinear FEA are illustrated in Figs. 9 and 10. It is shown in Fig. 9 that the force along the X-axis makes the lost motion along the Y-axis worse, and the worst point for the two-axis loading case occurs at the smallest force along the Y-axis. Figure 10 shows that the input stage's off-axis translation is less than 0.14% of the primary motion. Displacement difference (Y_{ay}–Y_{ay}') on the input stage along the Y-axis is captured in the nonlinear FEA and shown in Fig. 11. The cross-axis coupling error for the motion stage is shown in Fig. 12, of which the maximal value is less than 3.5% of the case without cross-axis coupling. It is also shown that the parasitic rotational yaw obtained from nonlinear FEA is lower than 7 urad (Fig. 13).

It is observed that the assumed rigid connecting bar produces non-trivial deformation in the nonlinear FEA (as shown in Figs. 10 and 14), which has introduced the non-isotropic characteristics between the two motion axes. This may be the main reason for the large discrepancy between the analytical model and the FEA model (Fig. 8). In addition, the nonlinear FEA results are limited by solver ability, meshing size and type etc, and therefore are not accurate in certain cases. From the qualitative analysis it is well know that the single-axis loading or the same two-axis loading generates no parasitic rotation (minimal rotation). However, Fig. 14 shows different results. For the single-axis loading case, the non-zero nonlinear FEA results are definitely not accurate. For the same two-axis loading, the nonlinear FEA results are not the minimal, which may be attributed to the FEA inaccuracy or the non-isotropic characteristics between the two motion axes. Considering the manufacturing imperfection for the 3D printed prototype and the limited resolution of the displacement sensor, it is not sure to judge which

theoretical model (analytical/FEA) is more accurate at this stage based on the initial testing results.

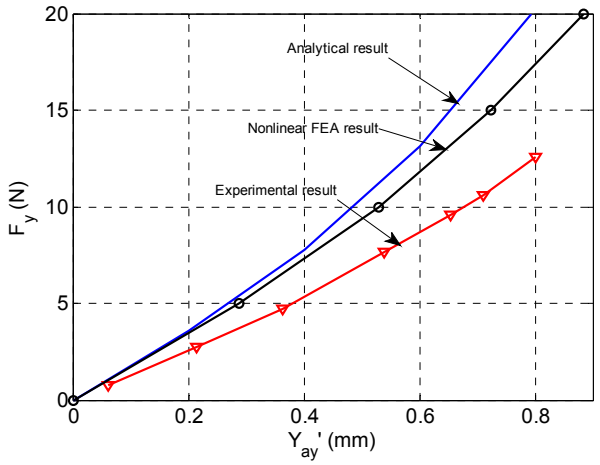

Figure 8 Relationship between the single-axis loading along the Y-axis and the input stage displacement

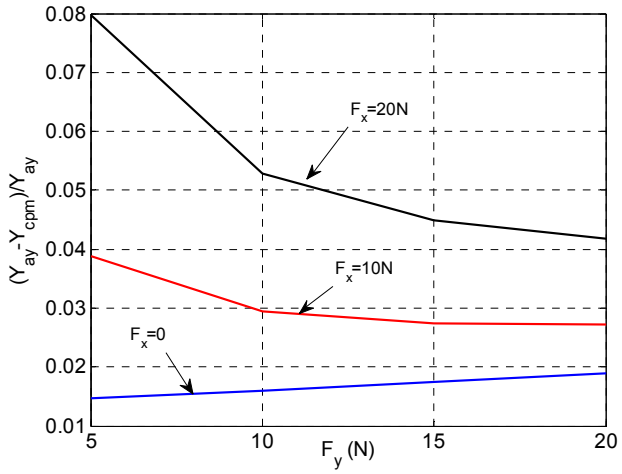

Figure 9 Lost motion from nonlinear FEA along the Y-axis

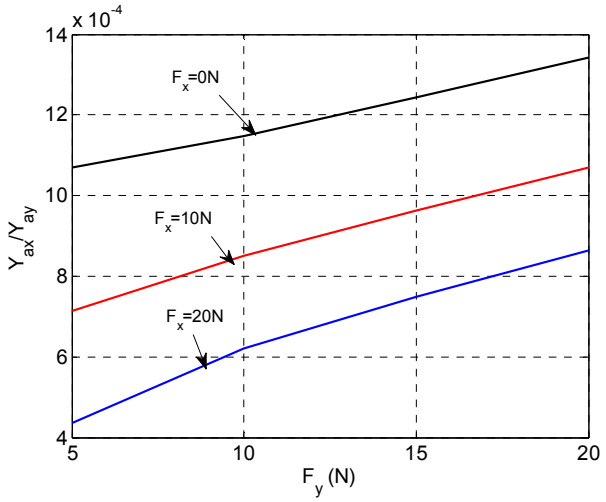

Figure 10 Input stage's off-axis displacement from nonlinear FEA along the Y-axis

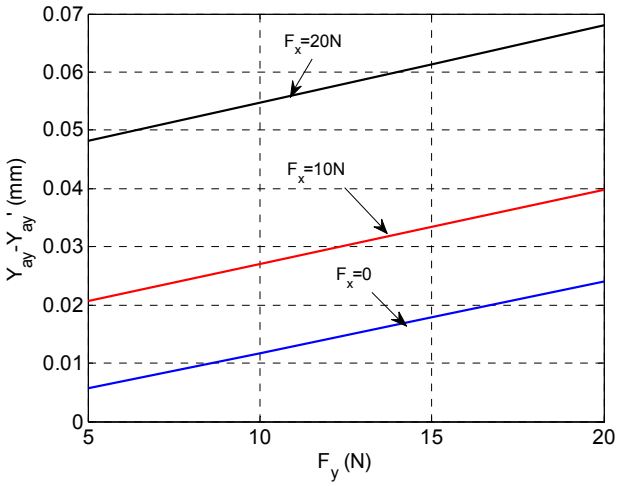

Fig. 11 Displacement difference on the input stage along the Y-axis

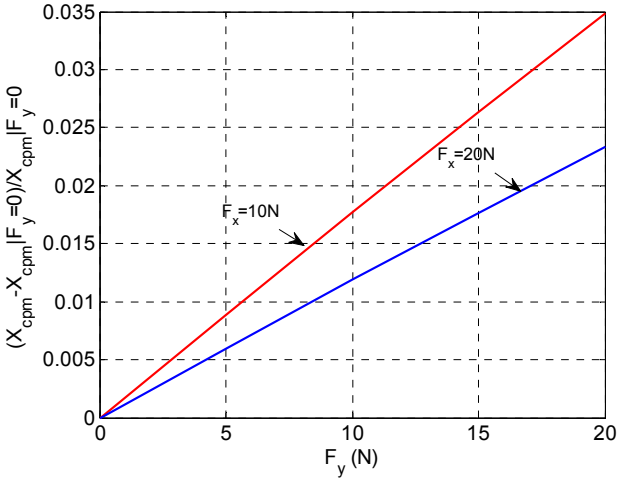

Figure 12 Cross-axis coupling error of the motion stage along the X-axis

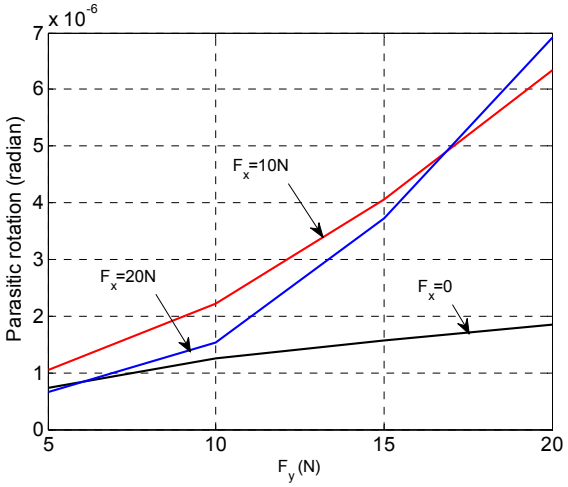

Fig. 13 Parasitic rotation of the motion stage

Figure 15 shows the 5-order natural modal shapes obtained from FEA with the first two-order ones for the two primary translations in plane. The lowest natural frequency is 100.98 Hz along the Y-axis. The natural frequencies along the X- and Y-axes are not exactly same

since the motion mass (i.e. the connecting bar's mass) in each axis differs.

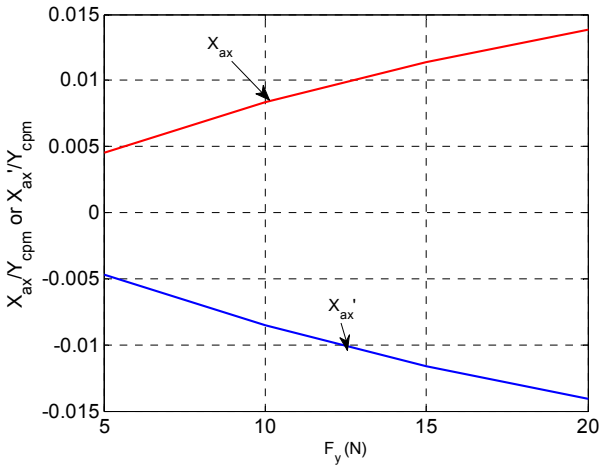

Fig. 14 Cross-axis motion of the input stage of the X-axis under single-axis loading along the Y-axis

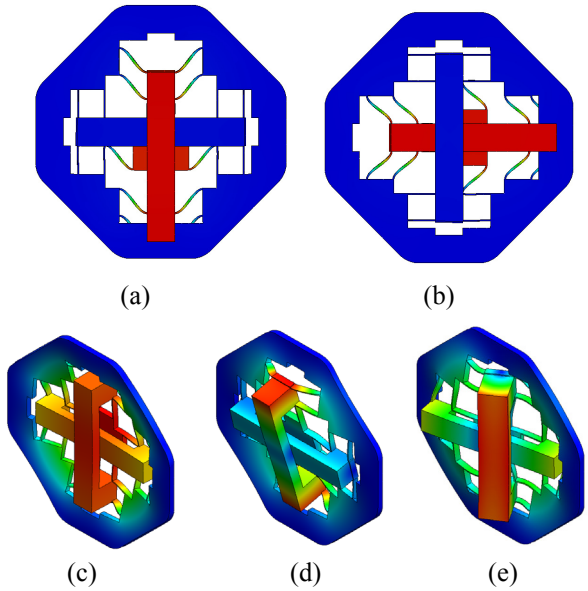

Figure 15 Natural modal shapes from FEA: (a) modal frequency 100.98 Hz; (b) modal frequency 112.88 Hz; (c) modal frequency 209.34 Hz; (d) modal frequency 296.05 Hz; (e) modal frequency 300.43 Hz

5 Discussions

Despite some improvements for the proposed novel 4-PP XY CPM over the existing designs, there are still some exposed tradeoffs. Due to the use of BPMs, large load-stiffening effect is introduced. This negative effect will reduce the motion range of the mechanism, which is limited by the buckling load and the large stress level. Here, the large stress is contributed from the significant tension in addition to the bending.

Although monolithic fabrication can be done by the 3-D printer as mentioned above, but considering the manufacturing precision requirements and material property, assembly should be adopted for the novel 4-PP XY CPM. One can fabricate the planar XY CPM without the connecting bars at first from a piece of aluminum alloy plate using the EDM (electrical discharge machining) or water cutting, and then fabricate the two *very rigid* connecting bars before the final assembly between the planer XY CPM and the connecting bars. A high-precision testing system for the assembled prototype is needed for verify the analytical models and characterize the system performances in the future.

The analytical models provided in Section 3 can be further improved. On the one hand, a more accurate model for the tensile force in Eq. (1) can be used for extending the accuracy range instead of the current first-order model for the tensile force. On the second hand, the assumptions mentioned earlier such as ignored rotational effect, no lost motion, and zero input stage's off-axis displacement, need to be removed to consider more practical models.

Note that the modal frequencies can be further enhanced by increasing the beam number using elastic average in the BPM without worsening the motion range. In order to attenuate the load-stiffening effect from the BPMs, a better-behaving exactly-constrained compliant P joint [14] can then be employed to replace each BPM in the 4-PP XY CPM.

6 Conclusions

A novel 4-PP XY CPM with a new topology structure has been developed. Its analytical model has been derived and also compared with the FEA and experiment result.

The novel 4-PP XY CPM, composed of exactly-constrained compliant mechanisms (BPMs) has a compact configuration, good dynamics, well-constrained parasitic rotation and cross-axis coupling of the motion stage, completely eliminated cross-axis motion of the input stage, and reduced lost motion.

It is expected that the proposed new topology structure can be extended to design the fully symmetrical spatial translational CPMs through rigidly connecting each two compliant P joints on the base in the two non-adjacent legs.

Acknowledgements

Mr. Tim Power and Mr. Michael O'Shea in University College Cork are greatly appreciated for their works on the 3-D printing and prototype initial testing.

References

1. Schitter, G., Thurner, P.J, and Hansma, P.K., 2008, "Design and Input-Shaping Control of a Novel Scanner for High-Speed Atomic Force Microscopy", *Mechatronics*, 18:282-288.
2. Werner, C., Rosielle, P.C.J.N., and Steinbuch, M., 2010, "Design of a Long Stroke Translation Stage for AFM", *International Journal Machine Tools and Manufacture*, 50(2):183-190.
3. Gorman, J.J., and Dagalakis, N.G., 2003, "Force Control of Linear Motor Stages for Microassembly", *ASME International Mechanical Engineering Conference and Exposition*, Washington, DC, Nov. 15–21, USA.
4. Vettiger, P., Despont, M., Drechsler, U., Durig, U., Haberle, W., Lutwyche, M.I., Rothuizen, H. E., Stutz, R., Widmer, R., and Binnig, G. K., 2000, "The Millipede—More Than One Thousand Tips for Future AFM Data

Storage", *IBM Journal of Research and Development*, 44(3):323–340.

5. Howell, L.L., 2001, *Compliant Mechanisms*, Wiley, New York.
6. Awtar, S., and Slocum, A.H., 2007, "Constraint-Based Design of Parallel Kinematic XY Flexure Mechanisms", *ASME Journal of Mechanical Design*, 129(8):816–830.
7. Awtar, S., Ustick, J., and Sen, S., 2012, "An XYZ Parallel Kinematic Flexure Mechanism with Geometrically Decoupled Degrees of Freedom", *ASME Journal of Mechanisms and Robotics*, 5(1):015001
8. Hao, G., 2014, "A 2-legged XY Parallel Flexure Motion Stage with Minimized Parasitic Rotation", *Proceedings of the IMechE, Part C: Journal of Mechanical Engineering Science*. DOI: 10.1177/0954406214526865
9. Hao, G. and Kong, X., 2012, "Novel XY Compliant Parallel Manipulators for Large Translation with Enhanced Out-of-plane Stiffness", *ASME Journal of Mechanical Design*, 134: 061009.
10. Sun, X., Chen, W., Zhou, R., Chen, W., and Zhang, J., 2014, "A Decoupled 2-DOF Flexure-Based Micropositioning Stage with Large Travel Ranges", *Robotica*. DOI: 10.1017/S0263574713000969
11. Li, Y., Xiao, S., Xi, L., and Wu, Z., 2014, "Design, Modeling, Control and Experiment for a 2-DOF Compliant Micro-motion Stage," *International Journal of Precision Engineering and Manufacturing*, 15(4):735-744, 2014.
12. Olfatnia, M., Sood, S., Gorman, J., and Awtar, S., 2013, "Large Stroke Comb-drive Actuators based on the Clamped Paired Double Parallelogram Flexure", *IEEE/ASME Journal of Micro Electro Mechanical Systems*, 22(2):483-494. DOI: 10.1109/JMEMS.2012.2227458
13. Awtar, S., and Slocum, A.H., 2007, "Characteristics of Beam-Based Flexure Modules", *ASME Journal of Mechanical Design*, 129 (6): 624-639.
14. Hao, G., Meng, Q., and Li, Y., 2013, "Design of Large-range XY Compliant Parallel Manipulators Based on Parasitic Motion Compensation", *Proceedings of the ASME 2013 International Design Engineering Technical Conferences & Computers and Information in Engineering Conference*, August 4–7, 2013, Portland, Oregon, USA. DETC2013–12206.